Available online at www.sciencedirect.com

SCIENCE DIRECT®

Journal of African Earth Sciences 40 (2004) 147–161

Journal of African Earth Sciences

www.elsevier.com/locate/jafrearsci

Sedimentology and taphonomy of the upper Karoo-equivalent Mpandi Formation in the Tuli Basin of Zimbabwe, with a new $^{40}Ar/^{39}Ar$ age for the Tuli basalts

Raymond R. Rogers [a,*], Kristina Curry Rogers [b], Darlington Munyikwa [c], Rebecca C. Terry [d], Bradley S. Singer [e]

[a] *Department of Geology, Macalester College, 1600 Grand Avenue, St. Paul, MN 55105, USA*
[b] *Science Museum of Minnesota, 120 W. Kellogg Boulevard, St. Paul, MN 55102, USA*
[c] *National Museum of Natural History, Box 240, Bulawayo, Zimbabwe*
[d] *Department of the Geophysical Sciences, University of Chicago, 5734 South Ellis Avenue, Chicago, IL 60637, USA*
[e] *Department of Geology and Geophysics, University of Wisconsin-Madison, 1215 W Dayton Street, Madison, WI 53706, USA*

Received 8 March 2004; received in revised form 6 October 2004; accepted 12 November 2004

Abstract

Karoo-equivalent rocks in the Tuli Basin of Zimbabwe are described, with a focus on the dinosaur-bearing Mpandi Formation, which correlates with the Elliot Formation (Late Triassic–Early Jurassic) in the main Karoo Basin. Isolated exposures of the Mpandi Formation along the banks of the Limpopo River consist of red silty claystones and siltstones that preserve root traces, small carbonate nodules, and hematite-coated prosauropod bones. These fine-grained facies accumulated on an ancient semi-arid floodplain. Widespread exposures of quartz-rich sandstone and siltstone representing the upper Mpandi Formation crop out on Sentinel Ranch. These strata preserve carbonate concretions and silicified root casts, and exhibit cross-bedding indicative of deposition via traction currents, presumably in stream channels. Prosauropod fossils are also preserved in the Sentinel Ranch exposures, with one particularly noteworthy site characterized by a nearly complete and articulated *Massospondylus* individual.

An unconformity caps the Mpandi Formation in the study area, and this stratigraphically significant surface rests on a laterally-continuous zone of pervasive silicification interpreted as a silcrete. Morphologic, petrographic, and geochemical data indicate that the Mpandi silcrete formed by intensive leaching near the ground surface during prolonged hiatus. Chert clasts eroded from the silcrete are intercalated at the base of the overlying Samkoto Formation (equivalent to the Clarens Formation in the main Karoo Basin), which in turn is overlain by the Tuli basalts. These basalts, which are part of the Karoo Igneous Province, yield a new $^{40}Ar/^{39}Ar$ plateau age of 186.3 ± 1.2 Ma.

Keywords: Karoo; Silcrete; Unconformity; Taphonomy; Dinosaurs; $^{40}Ar/^{39}Ar$ age

1. Introduction

The Karoo Basin of South Africa preserves a spectacular succession of Upper Carboniferous–Lower Jurassic rocks of sedimentary and volcanic origin collectively referred to as the Karoo Supergroup. These rocks span several kilometers in thickness, and they reflect evolving depositional systems and shifting palaeoclimatic regimes in the fill history of a retroarc foreland basin. Decades of dedicated research have shed considerable light on the nature and complexity of the Karoo Basin, which played a central role in the geological

* Corresponding author. Tel.: +1 651 696 6434; fax: +1 651 696 6122.
E-mail address: rogers@macalester.edu (R.R. Rogers).

0899-5362/$ - see front matter © 2004 Elsevier Ltd. All rights reserved.
doi:10.1016/j.jafrearsci.2004.11.004

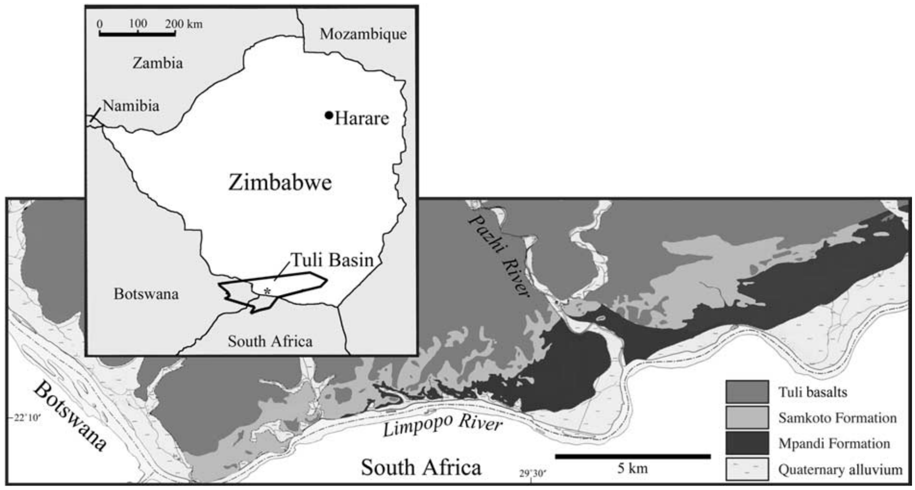

Fig. 1. Map of Karoo-equivalent units in the Limpopo study, southern Zimbabwe, showing the generalized outcrop belt of the Mpandi and Samkoto formations and overlying Tuli basalts (compiled and modified from the 1:100,000 Mazunga and Tuli sheets of the Geological Survey of Rhodesia, 1974). Inset map shows location of study area (asterisk) within the Tuli Basin.

history of Gondwana (Dingle et al., 1983; Johnson et al., 1997; among many others). In recent years, the focus has expanded to include related sedimentary depocentres outside of the main Karoo, such as the Tuli Basin, which occupies the common border regions of Botswana, Zimbabwe, and South Africa (Fig. 1). Recent work on Karoo-equivalent strata in the South African portion of the Tuli Basin has clarified the sedimentology of a suite of terrestrial palaeoenvironments, and led to the establishment of a refined stratigraphic framework (Bordy, 2000; Bordy and Catuneanu, 2001, 2002a,b,c).

This report examines the geology of Karoo-equivalent strata in the Zimbabwean part of the Tuli Basin, which has remained relatively unexplored. The focus is on the Mpandi Formation (Cooper, 1980), which correlates with the Elliot Formation (Late Triassic–Early Jurassic) in the main Karoo Basin and the informal "Upper Unit" of Bordy and Catuneanu (2001) in the South African part of the Tuli Basin. New data pertaining to the sedimentology and taphonomy of the Mpandi Formation is presented, and a laterally extensive unconformity that caps the unit throughout the study area is described. This previously unrecognized unconformity is directly underlain by a continuous zone of pervasive silicification interpreted as a silcrete that presumably formed in response to prolonged hiatus and intensive leaching in an environment that was becoming increasingly arid. In addition, a new $^{40}Ar/^{39}Ar$ age for the Tuli basalts, which overlie Karoo-equivalent sedimentary deposits, is reported. This new age represents the first radioisotopic analysis of the Tuli basalts in Zimbabwe.

2. Study area and methods

The study area is located approximately 45 km to the west of the border town of Beitbridge, and is bound to the south by the Limpopo River (marking the international boundary with South Africa) (Fig. 1). Exposures of the Mpandi Formation crop out on Sentinel Ranch in the vicinity of the confluence of the Pazhi and Limpopo rivers. All outcrops of the Mpandi Formation and the overlying Samkoto Formation in this region were studied, and these two units were tracked to the east to Nottingham Ranch, where deposits of the underlying Gushu and Fultons Drift Formations are exposed.

Ten stratigraphic sections were measured to provide a framework for sampling and a basis for facies analysis. Thin sections were utilized to explore mineralogy and micromorphology. X-ray fluorescence (XRF) was used to determine major and trace element concentrations through the upper Mpandi Formation and into the capping silcrete. Beads and pellets were analyzed using a Philips PW 2400 XRF spectrometer with a Rhodium (Rh) X-ray source.

Taphonomic data that pertain to basic modes of preservation were also collected in the field (e.g., observations on fossil abundance, skeletal articulation, element association, orientation, and breakage). Selected fossil bones were collected and analyzed to determine permineralizing agents using petrographic microscopy and a Zeiss DSM 960 scanning electron microscope (SEM) with an energy dispersive spectrometer (EDS). Polished thin sections were coated with carbon and analyzed at 20 kV and 30 μA. Authigenic mineral fills were documented with high-resolution backscatter-electron images.

3. General geological setting

3.1. Karoo Basin

Collision of the palaeo-Pacific and Gondwanan plates resulted in the formation of the Cape Fold Belt and the genetically coupled Karoo Basin in southern Africa, and this extensive tectonically partitioned foreland basin filled with up to 12 km of terrestrial and marine strata ranging in age from Late Carboniferous to Early Jurassic (Smith et al., 1993; Johnson et al., 1996, 1997; Catuneanu et al., 1998). Sedimentary rocks in the main Karoo Basin of South Africa are subdivided into four major lithostratigraphic units that reflect shifting tectonic and climatic regimes through time. In ascending order, they include the Dwyka, Ecca, Beaufort, and informal "Stormberg" Groups. These units are exposed across vast tracts of South Africa, and they have been intensely studied from both a sedimentological and a palaeontological perspective (e.g., Broom, 1912; Haughton, 1924; Kitching, 1977; Kitching and Raath, 1984; Smith et al., 1993; Rubidge et al., 1995; Johnson et al., 1996; Hancox and Rubidge, 1997; Smith and Kitching, 1997; Catuneanu et al., 1998; Bordy et al., 2004). Basalts of the Drakensberg Group cap Karoo deposits in South Africa and signal the end of Karoo sedimentation. Recent analyses (Duncan et al., 1997) indicate a late Early Jurassic eruptive history for these basalts.

3.2. Tuli Basin

Karoo-equivalent rocks are less well known to the north in Zimbabwe, where they are essentially confined to localized basins in the Zambezi and Limpopo river valleys (Thompson, 1975). The Tuli Basin, which trends roughly east-west for ~300 km in the shared border region of South Africa, Zimbabwe, and Botswana (Fig. 1), preserves an estimated thickness of 450–500 m of strata (Bordy, 2000; Bordy and Catuneanu, 2001, 2002a,b,c). It has been interpreted as the down-dropped western arm of a failed triple junction related to the break-up of Gondwana (Vail et al., 1969; Burke and Dewey, 1973). However, an episode of mid-Jurassic rifting and associated subsidence fails to accommodate the substantial record of pre-Jurassic strata preserved in the basin. Accordingly, Catuneanu et al. (1999) proposed that the Tuli Basin reflects, at least in part, tectonic flexure and subsidence in the back-bulge region of the Karoo foreland that commenced in the Late Palæozoic–Early Mesozoic. Bordy and Catuneanu (2001, 2002a,b,c) provide detailed descriptions and interpretations of the fluvial and aeolian strata that comprise the Karoo Supergroup in the South African portion of the Tuli Basin.

3.3. Stratigraphic overview

In the Zimbabwean portion of the Tuli Basin strata equivalent to the Karoo Supergroup crop out along the valley of the Limpopo River (Fig. 2). In ascending stratigraphic order, the following sedimentary units

Karoo Basin (main) (Johnson, 1994)		**Tuli Basin South Africa** (Bordy and Catuneanu, 2001, 2002a)	**Tuli Basin Zimbabwe** (Thompson, 1975)	**Tuli Basin Zimbabwe** (Cooper, 1980)
"Stormberg Group"	Clarens Formation	Clarens Formation	"Forest Sandstone"	Samkoto Formation
	Elliot Formation	Upper Unit	Red Beds	**Mpandi Formation**
	Molteno Formation	Middle Unit*	"Escarpment Grit"	Gushu Formation
Beaufort Group		Middle Unit*		
Ecca Group		Basal Unit (undifferentiated)	Fulton's Drift Mudstones	Fulton's Drift Formation
Dwyka Group			Basal Beds (undifferentiated)	Dwyka diamictite

Fig. 2. Lithostratigraphic schemes for Karoo strata in South Africa (Johnson, 1994, main Karoo Basin; Bordy and Catuneanu, 2001, 2002a, Tuli Basin) and Zimbabwe (Thompson, 1975, Cooper, 1980; Tuli Basin). Bordy and Catuneanu (2001) proposed two potential correlations of the Middle Unit (marked with asterisk) in the Tuli Basin of South Africa. In this report we follow the stratigraphic nomenclature of Cooper (1980).

Fig. 3. (a) Outcrop view of Tuli basalts, which attain a thickness of approximately 3 m in the study area. (b) The Tuli basalt is characterized by a devitrified glass matrix that contains acicular iron–titanium oxide crystals and olivine crystals. Scale bar = 7 mm.

are recognized in this ‘‘northern Karoo’’ depocentre (Thompson, 1975; Cooper, 1980; Munyikwa, 1997): (1) ‘‘Basal Beds’’ (undifferentiated), (2) Fultons Drift Formation, (3) Gushu Formation, (4) Mpandi Formation, and (5) Samkoto Formation. The Tuli basalts overlie these sedimentary deposits.

The base of the section is marked by an unconformity that separates underlying Precambrian granulite-gneiss from either localized erosional remnants of the ‘‘Basal Beds,’’ which consist of poorly sorted sandstones and conglomerates of presumed glacial origin (Thompson, 1975), or the Fultons Drift Formation. Dwyka-equivalent ‘‘Basal Beds’’ were not observed during our reconnaissance of the study area. However, approximately 12 m of the overlying Fultons Drift Formation were studied on Nottingham Ranch (22°07′52″ S, 29°41′26″ E). This formation, which purportedly attains a thickness of up to 120 m in the region (Thompson, 1975), consists locally of dark gray carbonaceous clayshales intercalated with beds of silty lignite. A 20-cm-thick reddish-brown sheet of conglomerate characterized by rounded pebbles of chert and silicified wood marks the contact between the Fultons Drift Formation and the overlying Gushu Formation. The local Gushu section on Nottingham Ranch consists of ~15 m of interbedded conglomerate and coarse-grained, cross-bedded sandstone.

The Mpandi Formation overlies the Gushu Formation, but unfortunately the intervening contact was not observed in the study area. Previous thickness estimates for the Mpandi Formation based on borehole data range up to 300 m (Thompson, 1975; Cooper, 1980). In our reconnaissance two discrete outcrop belts of the Mpandi Formation were identified and studied, and both are described below. The Mpandi Formation is in turn overlain by the Samkoto Formation (=Clarens Formation in the main Karoo Basin). The Samkoto Formation is widely exposed in the study area, where it consists of up to 20 m of fine-to-medium-grained pale brown (10YR 8/4) quartz-rich sandstone that weathers to a characteristic red colour (10R 5/6). The base of the Samkoto Formation exhibits chert rip-up clasts (derived from the underlying Mpandi silcrete, see below) and localized small- to medium scale tabular and trough cross-bedding. Faint large-scale cross-bedding of probable aeolian origin is developed in upper reaches of the unit. The red weathered surface of the formation tends to exfoliate into distinctive polygonal sheets.

The Tuli basalts cap the sedimentary succession in the study area (Fig. 3a). This aphanitic basalt is characterized by a devitrified glass matrix that contains acicular iron–titanium oxide crystals and euhedral olivine crystals that are partially altered by serpentine, and often fringed by iddingsite (Fig. 3b). Chlorite is present as an alteration product. Sub-vertical porphyritic dikes also crop out in the study area, and these are characterized by large plagioclase phenocrysts set in a fine-grained matrix of predominantly plagioclase, with lesser amounts of olivine, clinopyroxene, and iron–titanium oxides.

4. Sedimentology and taphonomy of the Mpandi Formation

4.1. Regional perspective

Working in nearby exposures in South Africa, Bordy and Catuneanu (2001, p. 607) reported an estimated thickness of ~200–280 m for the Mpandi-equivalent ‘‘Upper Unit,’’ with a ‘‘maximum exposed thickness’’ of 30 m in outcrop. The schematic stratigraphic profile used to illustrate the entire ‘‘Upper Unit’’ is ~17 m thick (Bordy and Catuneanu, 2001; their Fig. 3). This profile exhibits two alternating facies assemblages that are distinguished on the basis of grain size and sedimentary structures. The coarser grained ‘‘sandstone facies assemblage’’ was interpreted as the depositional product of wide and shallow ephemeral streams that experienced flash floods. The ‘‘fine-grained facies assemblage’’ was interpreted as the deposits of associated floodplains that aggraded under semi-arid conditions. The ‘‘Upper Unit’’ is capped by a silcrete horizon, which was described as laterally continuous and interpreted to pass conformably into the overlying aeolian facies of the

Clarens Formation (=Samkoto Formation) (Bordy and Catuneanu, 2001, 2002a).

Two general outcrop areas were studied on the Zimbabwean side of the border. Widespread exposures were investigated on Sentinel Ranch, where the Mpandi Formation is commonly found in contact with the overlying Samkoto Formation, and where the maximum exposed thickness of the unit is again approximately 30 m. A more isolated set of exposures spanning approximately 17 m was studied at a lower elevation along the banks of the Limpopo River, to the east of its confluence with the Pazhi River. These strata exhibit sedimentary characteristics consistent with relegation to the Mpandi Formation (see description below), but their exact position within the local section is difficult to ascertain given their isolated nature and the presence of nearby faults (Geological Survey of Rhodesia, 1974).

4.2. Sentinel Ranch exposures

A section through readily accessible outcrop of the Mpandi Formation (Sentinel Ranch: 22°09′45.1″ S, 29°28′32.6″ E) is schematically illustrated in Fig. 4a and described here in detail. This section includes 38 m of continuous exposure of the upper Mpandi Formation and part of the superjacent Samkoto Formation.

Red beds (7.5R 7/2) of fine-grained, moderately sorted, quartz-rich sandstone and siltstone crop out at the base of the Sentinel section. Although the basal few meters of the section appear massive, faint small-scale trough cross-bedding (~3 cm sets) is apparent approximately 2 m up-section. Trough cross-bed sets ranging from 5 to 20 cm in thickness are more prominent starting at approximately 6 m above the base of the section (Fig. 5a). Small stringers of red claystone rip-ups and white chert rip-ups (reworked silicified roots) mark some set boundaries. Some foresets also show development of thin red claystone partings. Light gray carbonate concretions and horizontally-trending silicified root casts with drab gray reduction halos are scattered throughout the exposures (Fig. 5b).

A 2.4 m thick and ~25 m wide bed of medium- to coarse-grained light gray (N 8/) sandstone crops out 9.6 m up-section. This strongly calcareous sandstone body has a 30–50 cm-thick basal lag of intraclast pebbles (chert, carbonate, claystone) and rare bone fragments (Fig. 5c). The basal lag is overlain by 20–40 cm-thick sets of trough cross-bedded sandstone, which are in turn capped by ripple cross-laminated deposits. A partial pelvis of a prosauropod dinosaur is preserved near the base of this sandstone lens. Another bed of fine- to medium-grained sandstone crops out 22.3 m up-section. This 2.3 m thick ledge of pale red (2.5 YR 7/2) calcareous sandstone is characterized by faint small-scale cross-bedding and localized horizontal bedding. Small scours draped with intraclast pebbles of

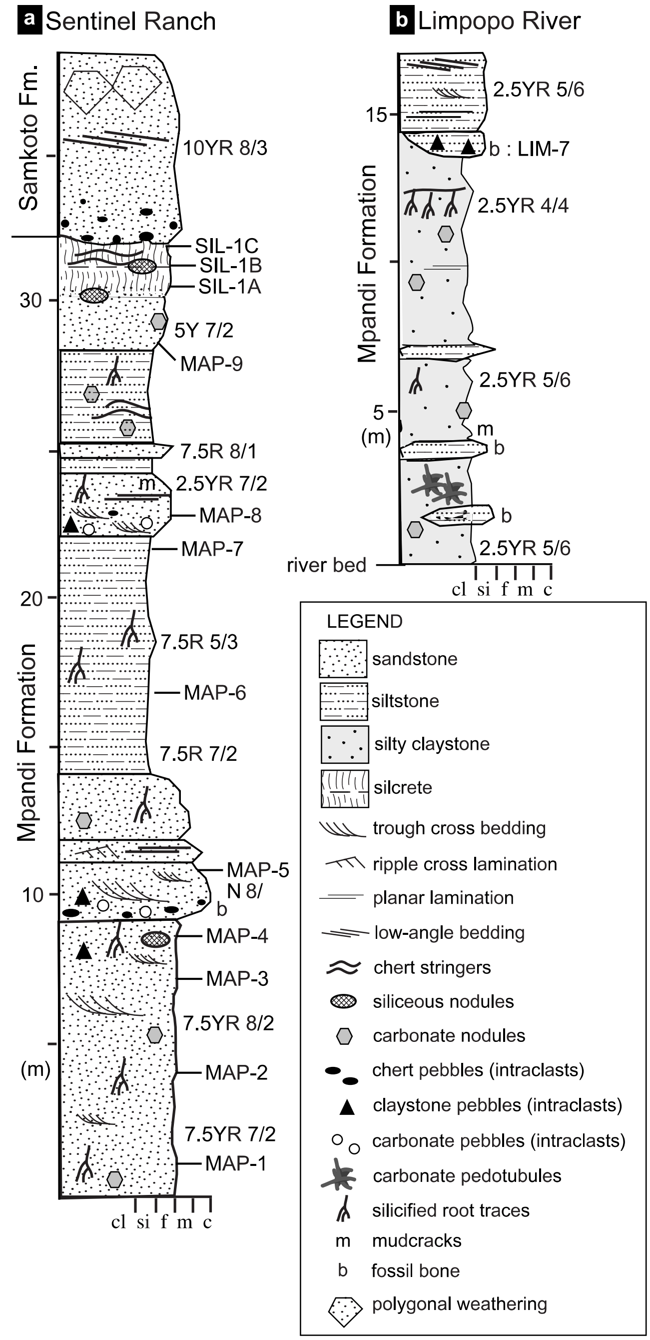

Fig. 4. (a) Schematic stratigraphic section measured through the upper Mpandi Formation and the base of the overlying Samkoto Formation on Sentinel Ranch (22°09′45.1″ S, 29°28′32.6″ E). This section spans 38 m of continuous exposure. Sample localities for XRF analyses (see Table 1) are indicated. (b) Schematic stratigraphic section spanning fine-grained exposures of the Mpandi Formation that crop out along the banks of the Limpopo River near its confluence with the Pazhi River (22°08′58.8″ S, 29°32′23.8″ E).

claystone, carbonate, and chert mark some set boundaries. In the upper half of the unit, red claystone partings locally delineate bedding, and some of these clay seams exhibit small mudcracks. Root mottling is developed near the top of the unit.

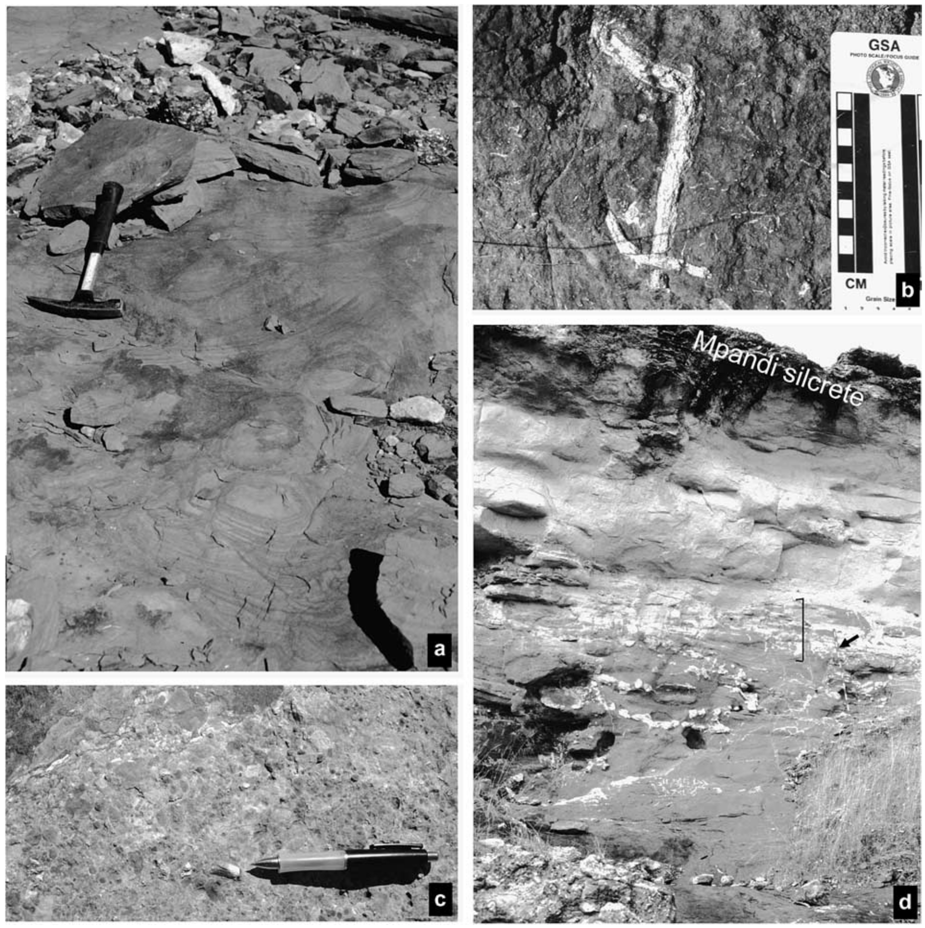

Fig. 5. Sedimentology of the Sentinel Ranch section (Fig. 4a). (a) Trough cross-bedding developed in fine-grained sandstone ~8 m above the base of the section. (b) Silicified roots and mm-scale rootlets are common. (c) Bone pebble (tip of pen) preserved in the midst of claystone, carbonate, and chert intraclasts at the base of a sandstone body ~10 m up-section. (d) The colour of the Mpandi Formation shifts from predominantly red to light gray (5Y 7/2) a few meters below the contact with the superjacent Samkoto Formation (bracket spans ~1 m thick zone of colour change). The top of the Mpandi Formation is characterized by pervasive silicification throughout the study area (Mpandi silcrete). Arrow points to Jacob's staff (10 cm increments).

The colour of the Mpandi Formation shifts from predominantly red to light gray (5Y 7/2) approximately 6 m below the contact with the superjacent Samkoto Formation throughout the Limpopo study area. This colour transition is interdigitating and irregular, and transpires over approximately 1 m of exposure (Fig. 5d). The upper gray beds consist of massive to faintly bedded siltstone that exhibits scattered siliceous root traces, irregular silica stringers, and siliceous concretions up to 10 cm in diameter. These concretions tend to increase in abundance up-section. The uppermost 1.5–2 m of the Mpandi Formation are characterized by pervasive silicification throughout the study area. This extensively silicified and heavily indurated cap, which is interpreted as a silcrete (Terry, 2001; Terry et al., 2001), is described in detail below.

Exposures of the upper Mpandi Formation show clear indication of deposition via traction currents (e.g., cross-bedding at various scales). Grain size trends (including the presence of conglomeratic "lag" facies), sedimentary structures, and stratal architecture suggest that the uppermost 30 m of the Mpandi Formation accumulated, at least in part, in active high-energy stream channels. Finer-grained sandstones and siltstones that exhibit root traces are interpreted to represent deposition in either: (1) low-energy and/or emergent portions of the channel belt, or (2) associated floodplain settings. Mpandi deposition culminated with a significant hiatus, during which the Mpandi silcrete formed.

4.3. Limpopo River exposures

Isolated exposures of the Mpandi Formation crop out along the Limpopo River immediately to the east of its confluence with the Pazhi River (22°08′58.8″ S, 29°32′23.8″ E: Figs. 4b, 6b). These localized outcrops, which span ~17 m of section, consist primarily of red

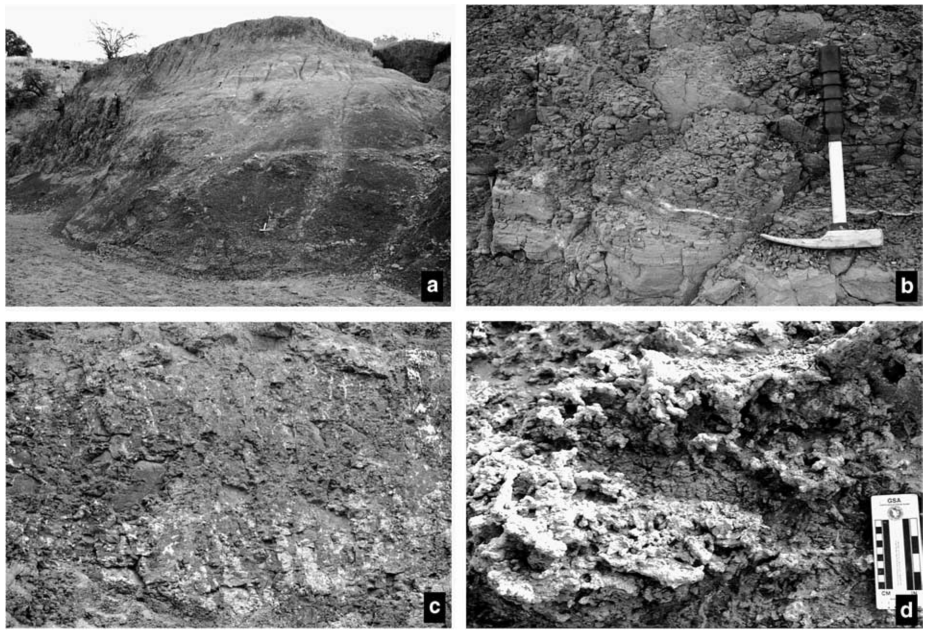

Fig. 6. (a) View of the Mpandi Formation along the Limpopo River. Approximately 17 m of fine-grained strata crop out near the confluence of the Limpopo and Pazhi rivers (Fig. 4b). (b) The local section is dominated by red silty claystones and siltstones that exhibit blocky parting. Thin beds and lenses of laminated siltstone (below hammer) crop out locally. (c) Mottling indicative of root traces is preserved in fine-grained beds of the Mpandi Formation. Root traces are typically small (<1 cm diameter) and vertical in orientation, and are delineated by drab (5Y 5/2) halos. (d) Localized clusters of calcareous pedotubules that exhibit an interwoven fabric are intercalated in the basal few meters of the section.

(2.5 YR 5/6) to mottled red and purple silty claystones and clay-rich siltstones that exhibit blocky parting and preserve root traces, small white carbonate nodules, and rare mudcracks. Scattered thin beds and lenses of planar laminated siltstone that occasionally exhibit basal load casts are also intercalated in the section (Fig. 6b). Root traces are typically small (<1 cm diameter) and vertical in orientation, and are delineated by drab (10GY 8/2) mottling (Fig. 6c). Localized clusters of calcareous pedotubules that exhibit an interwoven fabric are intercalated in the basal few meters of the section (Fig. 6d).

Facies of the Mpandi Formation exposed near the confluence of the Limpopo and Pazhi rivers are interpreted to represent deposition on an ancient semi-arid floodplain. Relatively dry, presumably semi-arid conditions during deposition are indicated by the red oxidized nature of the sediments, and the presence of carbonate nodules and $CaCO_3$-encrusted pedotubules.

4.4. Taphonomic observations

Munyikwa (1997) provided brief descriptions of several tetrapod localities in the Mpandi Formation, and reviewed the known tetrapod fauna. These localities were revisited during the course of this study, and new sites were discovered in both of the general outcrop areas described above (Sentinel Ranch and Limpopo River). At present, the majority of the known vertebrate localities in the Mpandi Formation are within a few tens of meters of the contact with the superjacent Samkoto Formation.

Most localities preserve the remains of single *Massospondylus* individuals (Munyikwa, 1997). Material is typically disarticulated, although one new locality (LIM-5: 22°09′44.4″ S, 29°28′17.1″ E) preserves nine articulated caudal vertebrae in association with a partially articulated hind limb and articulated pes. Another locality of interest is LIM-1 (22°09′28.2″ S, 29°29′43.8″ E: first described by Munyikwa, 1997), which preserves an exceptional skeleton with scant evidence of disturbance prior to final burial (Fig. 7a). The posterior half of a *Massospondylus* individual is exposed at the LIM-1 locality. The animal is resting on its back with intact hind limbs splayed symmetrically to each side. The caudal series is intact, although somewhat disjointed. Both ilia and partial right and left ischia are preserved, but both pubes are missing, and, in light of the specimen's supine position, are presumed lost to erosion upon exposure (as opposed to removed prior to burial). Three posterior dorsal ribs are exposed and remain in articulation, and there is the possibility that the front half of the skeleton is preserved and awaits excavation.

Bone of the LIM-1 specimen is light gray, with localized pink and purple staining. The quality of preservation is generally very good, with minor exfoliation of cortical bone due to modern weathering, and minor indication of lithostatic compaction. The specimen is preserved in light red (2.5 YR 6/2) fine-grained sandstone that appears predominantly massive. Small

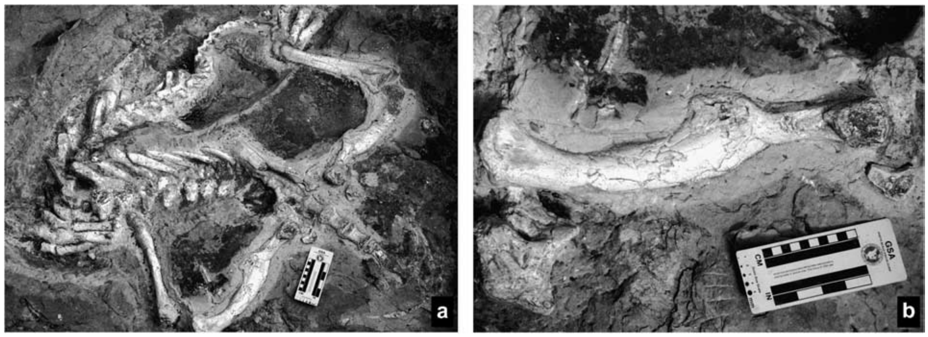

Fig. 7. (a) The posterior half of a single articulated *Massospondylus* individual is exposed at the LIM-1 locality. The animal is preserved in a supine position with intact hind limbs splayed symmetrically to each side. (b) Bone of the LIM-1 specimen is rimmed by a drab gray halo that varies from <1 to 10 cm in thickness. It is unknown whether this halo reflects localized reactions in the burial environment upon decay of soft tissues or a later diagenetic effect. The left femur is illustrated.

cross-bed sets (2–3 cm thick) were observed near the left pes, and flat clay pebbles and tiny silicified rootlets (1–3 mm diameter) occur in the encasing matrix. Thin clay partings are present immediately above the specimen. Interestingly, most of the specimen is rimmed by a drab gray halo that varies from <1 to 10 cm in thickness (Fig. 7b). It is unknown whether this halo reflects localized reactions in the burial environment upon decay of soft tissues or a later diagenetic effect. The LIM-1 locality is located 18 m beneath the Mpandi–Samkoto contact.

Another significant new locality (LIM-7: 22°08′59.6″ S, 29°32′23.7″ E) was discovered in Mpandi Formation exposures along the banks of the Limpopo River. LIM-7 is a promising new site that preserves the disarticulated remains of at least one prosauropod dinosaur. Bone at this locality was discovered in a 5 m-wide lens of reddish brown siltstone (2.5 YR 5/4) intercalated ~3 m below the top of local exposures (Figs. 4 and 8). The massive siltstone matrix of site LIM-7 is conglomeratic, and preserves abundant matrix-supported claystone pebbles of variable size. Bone was observed weathering from the base of the siltstone body along a several-meter-wide swath. A test pit confirmed the presence of abundant prosauropod bone. Several postcranial elements, including two partial ribs, a caudal vertebra and associated neural arch, a radius, a metapodial, and a phalanx, were exposed in an area comprising less than 1 m^2. Whether the site preserves the disarticulated remains of more than one individual is currently unknown (more thorough excavations are planned). The abundance of bone and the geometry of the deposit (a bone-filled lens

Fig. 8. The LIM-7 locality preserves the disarticulated bones of at least one prosauropod dinosaur. Skeletal debris is preserved in a siltstone lens intercalated ~3 m below the top of local exposures (white arrows delimit base). The deposit apparently accumulated in a localized meter-scale depression on the ancient Mpandi floodplain.

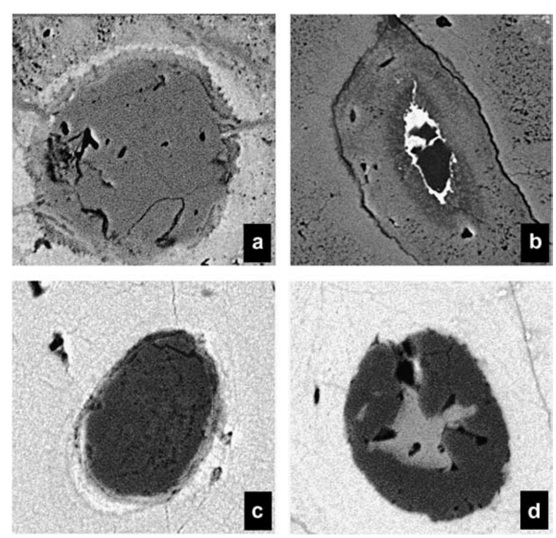

Fig. 9. Backscatter-electron images of authigenic fills in Mpandi bones. (a,b) SEM-EDS analyses of bones from the LIM-7 locality indicate that vascular canals and fractures tend to be filled with either calcite alone (image a, dark gray), or an initial thin coating of iron oxide (image b, light gray/white), followed by calcite (image b, dark gray). In rare cases vascular canals of bones from this locality are filled entirely with iron oxide. Patches of iron oxides are also evident in bone matrix. (c,d) SEM-EDS analyses of bones from the LIM-6 locality in the upper Mpandi Formation exhibit a different mode of permineralization. In most fills silica is the exclusive permineralizing agent (image c, dark gray). When calcite is present (image d, lighter gray), it is generally preceded by a silica phase (image d, darker gray).

within a palaeo-depression) are certainly suggestive of a multi-individual concentration (bonebed).

Bones preserved in the LIM-7 site are encrusted with a multi-mm thick rind of calcite and brown hematite. Cortical bone in contact with the rind exhibits abundant microfractures, and hematite-filled veinlets extend into bone interiors. Despite the macroscopic preponderance of hematite, thin section analysis indicates that calcite is the predominant permineralizing agent. SEM-EDS analyses indicate that vascular canals and fractures in LIM-7 bones are filled with either: (1) calcite alone, (2) an initial thin coating of iron oxide, followed by calcite, and more rarely (3) iron oxide alone (Fig. 9a and b). Patches of iron oxides are also evident in the bone matrix. Bone from LIM-6 (22°09′51.9″ S, 29°29′20.8″ E), a site in the upper Mpandi Formation, was analyzed for comparison. Thin section and SEM-EDS analyses of two elements from this site indicate that silica is the predominant permineralizing agent. In the relatively few cases where calcite is present, it is always preceded by a silica phase (Fig. 9c and d). Based on the abundant indication of silicification in the upper Mpandi Formation, it is likely that comparable cementation histories typify much of the fossil material in upper portions of the unit.

5. Mpandi silcrete

Silcretes are heavily indurated horizons of secondary silica accumulation typically composed of skeletal quartz grains set in a matrix of microcrystalline quartz or amorphous silica. The weight percent of silica in a true silcrete is generally greater than 90%. Silicification occurs by cementation and/or replacement of bedrock or unconsolidated sediment (Grant and Aitchison, 1970; Langford-Smith, 1978; Summerfield, 1983a; Webb and Golding, 1998; Milnes and Thiry, 1992). Sedimentary associations, field relationships, petrographic features, and geochemical data indicate that the Mpandi Formation is capped by a well-developed silcrete.

The Mpandi silcrete is a prominent indurated ledge developed throughout the study area, where it can be mapped for ~20 km along exposures that parallel the Limpopo River (Terry, 2001; Terry et al., 2001). It can also be traced across the border into South Africa (Bordy, 2000; Bordy and Catuneanu, 2001, 2002a). In outcrop, the ~1.5 m thick silcrete is characterized by abundant siliceous nodules, subhorizontal anastomosing siliceous stringers, and siliceous root traces. The degree of silicification visibly increases up-section (Fig. 10a). In upper portions of the silcrete, subhorizontal siliceous stringers increase in both length and thickness and coalesce to form thick resistant sheets that stand out in relief upon weathering (Fig. 10b). Sub-vertical cracks filled with chert cut through the network of subhorizontal stringers, and indicate multi-stage silicification. Pseudobrecciated textures are commonly developed near the top of the unit (Fig. 10c and d). Remnant primary bedding was not observed within the Mpandi silcrete.

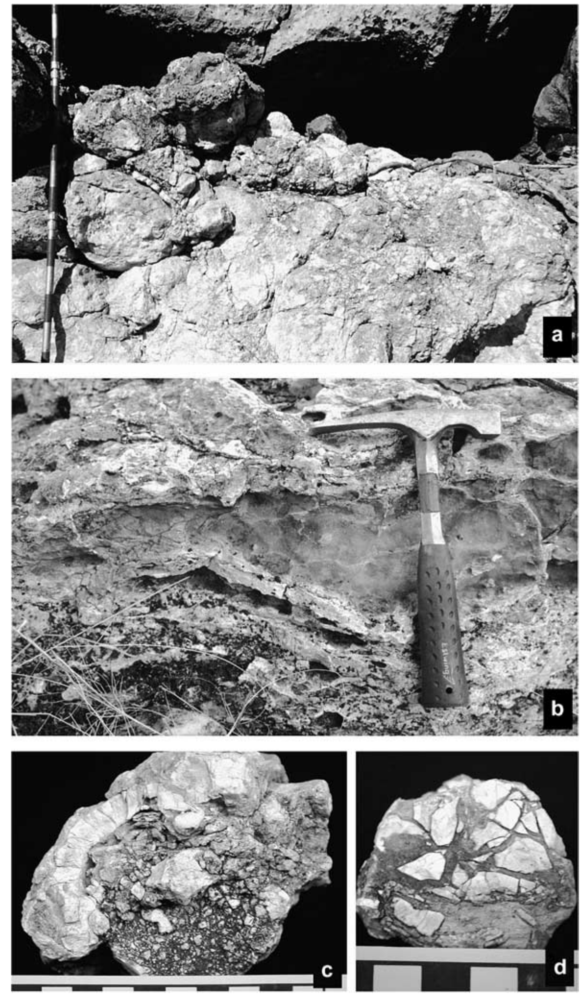

Fig. 10. (a) Exhumed top of Mpandi silcrete showing the disorganized and extensively altered nature of the horizon. (b) Subhorizontal siliceous stringers stand in relief near the top of the silcrete. (c,d) The top of the Mpandi silcrete is characterized by a pseudobrecciated texture.

5.1. Petrography

Fine-grained, moderately well-sorted quartz sandstone at the base of the silcrete exhibits intergranular voids filled with secondary silica. Microcrystalline quartz is present between primary skeletal grains, and in some instances appears to engulf these grains. The base of the Mpandi silcrete exhibits GS-fabric massive (grains supported, glaebules absent) to F-fabric (floating grains) with few glaebules or colloform features (for a complete review of terms see Summerfield, 1983b).

Distortion and obliteration of the host sediment is more apparent in samples derived from mid-portions of the silcrete (~1 m from top), although skeletal quartz grains and calcareous matrix are still preserved. Vein-fills that range in length from 0.75 to 1.5 cm and exhibit fine banding of length-fast chalcedony are common. These planar void fills can exhibit up to six distinct horizons of length-fast chalcedony, and occasionally show a more complex inward fill progression of microcrystalline quartz to length-fast chalcedony to macrocrystalline quartz (Fig. 11a). Some voids are entirely filled with microcrystalline quartz. At the top of the unit only traces of the original framework grains are preserved, and secondary silica blebs, glaebules, and veins are present in all orientations (Fig. 11b).

5.2. Geochemistry

Major and trace element concentrations were determined by X-ray fluorescence for a suite of samples from the Mpandi Formation and capping silcrete on Sentinel Ranch (Table 1). The Mpandi silcrete is clearly enriched in SiO_2 (89–99 wt.% SiO_2) relative to underlying sediments, which average 85 wt.% SiO_2. All other major element concentrations are depleted within the silcrete. A potential zone of accumulation is developed ~10 m beneath the base of the silcrete (samples MAP-6, MAP-7). Minor to trace amounts of Al, Fe, Ca, Mg, Na, K, and Ti within the Mpandi silcrete presumably reflect the minor presence of associated minerals such as calcite, anatese, albite, and remnant clays.

Trace element analysis of the upper Mpandi Formation and capping Mpandi silcrete reveals similar trends. All trace element concentrations are depleted in the uppermost portions of the silcrete, and most show increasing concentrations in lower portions of the silcrete, and in underlying strata. Again, there is an apparent zone of accumulation ~10 m beneath the silcrete.

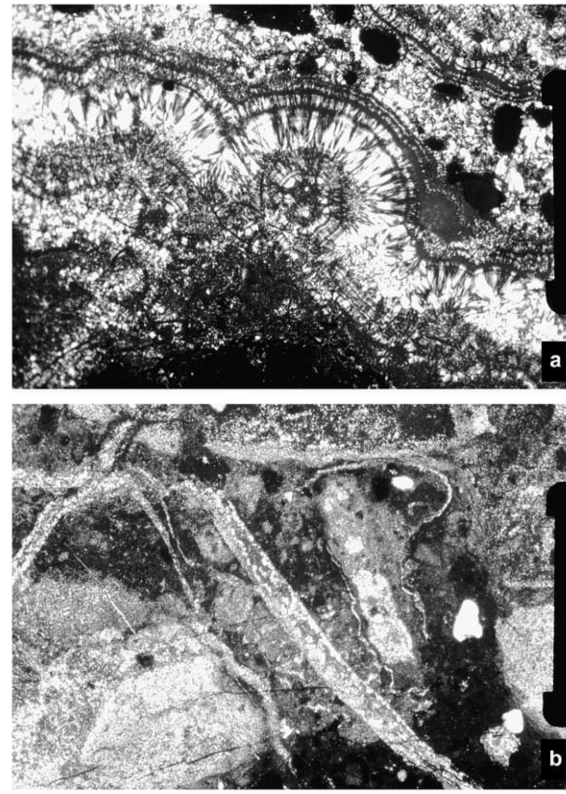

Fig. 11. (a) In thin section the Mpandi silcrete is characterized by abundant voids filled by multiple silica phases. In this view a planar void is filled with multiple length-fast chalcedony horizons and microcrystalline quartz. Scale bar = 7 mm. (b) At the top of the Mpandi silcrete silica blebs and veins are present in all orientations. Clastic skeletal grains comprise <5% of the rock. Scale bar = 3.5 mm.

5.3. Formative considerations

Thiry (1999) identified three general modes of silcrete formation: (1) groundwater silicification, (2) evaporation-based silicification, and (3) pedogenic silicification. Formation of the Mpandi silcrete at depth due to fluctuations of the Eh and pH of a silica-saturated water table

Table 1
Major and Trace element analyses of the upper Mpandi Formation and Mpandi silcrete

Sample	SiO_2	TiO_2	Al_2O_3	Fe_2O_3	MnO	MgO	CaO	Na_2O	K_2O	P_2O_5	LOI[a]	Total	Cr	Ba	V	Zr	Sr	Rb	Sc
MAP-1	83.44	0.32	8.73	1.48	0.01	0.68	1.05	1.84	2.31	0.05	0.05	99.96	18	860	19	354	108	82	5
MAP-2	87.25	0.17	5.34	0.63	0.05	0.35	4.09	1.12	1.55	0.03	0.04	100.62	12	1860	14	237	192	54	5
MAP-3	82.52	0.32	9.41	1.91	0.01	0.80	0.37	1.67	2.67	0.04	0.03	99.75	49	561	27	340	102	97	6
MAP-4	87.76	0.21	6.69	1.03	0.01	0.55	0.67	1.25	2.02	0.04	0.03	100.26	17	977	18	264	88	70	5
MAP-5	90.55	0.19	3.58	0.22	0.05	0.14	3.67	0.64	1.45	0.03	0.04	100.56	13	823	19	357	146	42	4
MAP-6	78.74	0.39	8.82	1.98	0.03	0.87	5.31	1.30	2.97	0.06	0.06	100.53	44	507	22	339	118	103	7
MAP-7	85.38	0.45	7.55	1.47	0.01	0.74	0.37	1.28	2.57	0.04	0.02	99.88	27	977	26	696	102	90	5
MAP-8	85.03	0.21	3.99	0.22	0.10	0.23	9.22	0.89	1.52	0.03	0.07	101.51	16	369	6	331	171	43	5
MAP-9	83.65	0.35	7.91	1.49	0.01	2.02	0.38	1.01	2.80	0.05	0.03	99.7	39	569	95	230	90	82	6
SIL-1A	89.47	0.23	3.95	0.58	0.00	1.42	0.30	0.49	1.36	0.04	2.25	100.06	44	369	19	265	66	33	4
SIL-1B	94.91	0.10	1.96	0.28	0.00	0.34	0.51	0.18	0.70	0.07	2.06	101.10	45	301	6	104	60	15	4
SIL-1C	98.58	0.03	0.72	0.17	0.00	0.03	0.22	0.00	0.20	0.04	1.17	101.16	18	117	5	46	36	8	4

Sampled horizons are indicated on Fig. 4a. Major element values in weight percent, trace element values in parts per million.
[a] LOI=Loss on ignition expressed as percent.

is inconsistent with general morphological characteristics and petrographic data. Subsurface silcretes tend to occur in lenses or pods, typically show a simple micromorphology, and are often associated with well-developed illite or kaolinite profiles (Nash et al., 1994; Simon-Coincon et al., 1996; Ullyott et al., 1998). The Mpandi silcrete, however, is a laterally extensive sheet that is not associated with any significant clay development and is characterized by complex void fills of length fast chalcedony, microquartz, and macroquartz.

Formation of the Mpandi silcrete due to evaporation is not supported by geochemical data. In the evaporative scenario, which has been implicated for silcretes in the Kalahari Desert (Nash et al., 1994), pore-waters bearing dissolved components move to the surface in an alkaline pan setting, salinity increases, and precipitation occurs. In this formative scenario, soluble elements such as Ca, Na, and K would be brought to the surface due to the upward migration of pore-water, resulting in an increase in salinity. Enrichment in both soluble major and trace elements would be expected within the silcrete. Geochemical trends within the Mpandi silcrete indicate the opposite—soluble elements such as Ca, Na, and K are clearly depleted within the Mpandi silcrete relative to underlying strata.

Terry et al. (2001) concluded on the basis of morphologic, petrographic, and geochemical data that the Mpandi silcrete most likely formed near the ground surface as a result of pedogenic processes. Extended weathering presumably prompted intensive leaching, and most elements were transported downward into underlying deposits (Table 1). Even Zr, which is generally immobile over a wide pH range, appears to have been leached from the silcrete. Translocation of most elements resulted in the relative enrichment of silica, which precipitated in a variety of forms and replaced the bulk of the host sediment. Whether additional silica was introduced from outside sources is unknown.

5.4. Indication of unconformity

The contact between the Mpandi Formation and the superjacent Samkoto Formation bears indication of both extended hiatus and erosion. With regard to evidence of hiatus, it is generally assumed that near surface silicification requires prolonged subaerial exposure of a relatively stable land surface (Milnes and Thiry, 1992; Smith et al., 1997; Thiry, 1999). The authigenic silica fabrics characteristic of well-developed silcretes take considerable time to develop, with estimates on the order of 10^5–10^6 years (Meyer, 1997). The Mpandi silcrete is a well-developed horizon characterized by a complex history of authigenic silicification (see Figs. 10 and 11). It caps a sedimentary succession that exhibits abundant evidence of pedogenesis, but none of the underlying palaeosols show comparable degrees of development. The silcrete is unique within the exposed Mpandi section, and its position at the very top of the formation indicates that deposition culminated with a protracted episode of landscape stability and subaerial weathering.

With regard to evidence of erosion, the sharp Mpandi–Samkoto contact (Fig. 12a) separates a heavily silicified bed of silcrete from overlying sandstone (Figs. 10a and 12a and b). At the outcrop scale the surface is generally planar, but locally it exhibits decimeter-scale relief that follows the irregular topography of the underlying

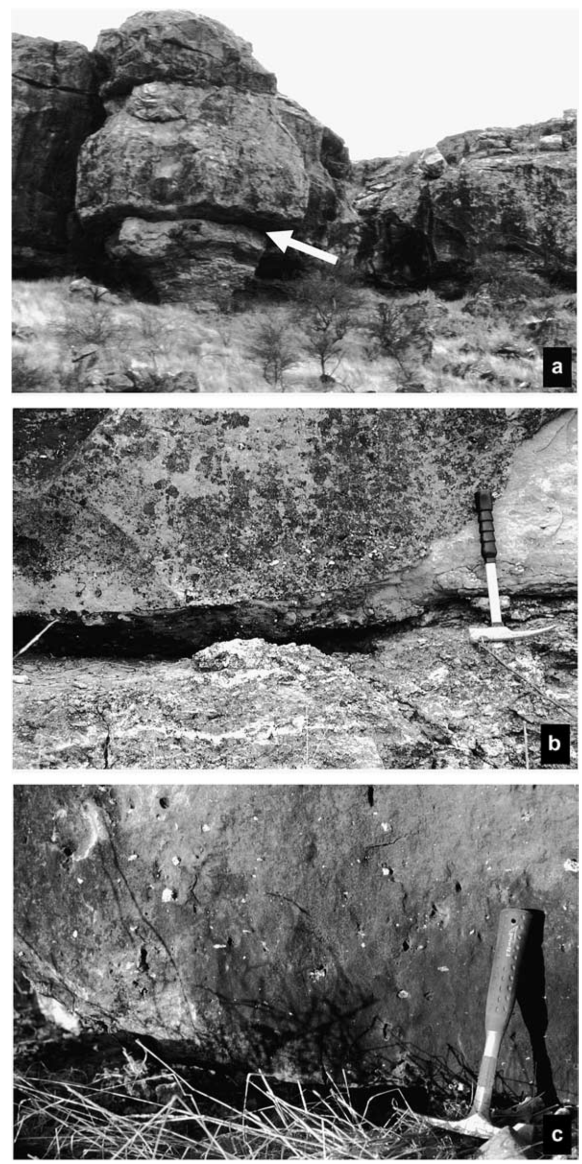

Fig. 12. (a) Outcrop view of the Mpandi–Samkoto boundary illustrating the sharp nature of contact (marked by arrow). Sandstone facies of the basal Samkoto Formation overlie a well-developed ledge-forming silcrete throughout the available outcrop belt. (b,c) Close-up views of contact showing evidence of erosion. In photograph b the Mpandi silcrete shows evidence of exhumation. In both views angular chert clasts derived from the Mpandi silcrete are intercalated at the base of the Samkoto Formation.

silcrete. The relatively limited relief on the contact presumably reflects, at least in part, the indurated nature of the silcrete, which would have definitely inhibited down-cutting. Chert clasts derived via exhumation and erosion of the silcrete are incorporated into basal deposits of the Samkoto Formation (Fig. 12b and c). These matrix-supported chert clasts are subangular, and show no evidence of imbrication. Clast size diminishes upward, ranging from 5 cm (long axis) at the base of the unit to ⩽5 mm (long axis) in upper reaches of the clast-bearing zone, which spans ~1.5 m.

6. New $^{40}Ar/^{39}Ar$ age for the Tuli basalts

Here a new $^{40}Ar/^{39}Ar$ age for the Tuli basalts is reported. This new age represents the first radioisotopic analysis of the Tuli basalts in Zimbabwe. Prior to this study, the age of Karoo-equivalent rocks in the Zimbabwe portion of the Tuli Basin was based on biostratigraphic data, with both tetrapods and fossil plants consistent with the section spanning the Permian–Early Jurassic (Thompson, 1975; Kitching and Raath, 1984). Working nearby in eastern Botswana, Aldiss et al. (1984) dated the "Stormberg Lavas" (=Tuli basalts) using K-Ar methods and concluded that they were probably older than 181 ± 4 Ma.

6.1. Sampling and analytical methods

A fresh sample of the Tuli basalt was collected on Sentinel Ranch (22°08′12.5″ S, 29°31′27.5″ E) from the base of the flow section, 50 cm above the top of the Samkoto Formation. From this sample a phenocryst-free groundmass separate was isolated from the 180–250 μm size fraction by standard crushing, magnetic, and hand-picking techniques. A 10 mg packet of these groundmass grains, each weighing about 1 mg, was irradiated for 50 h in the Cadmium-Lined In-Core Irradiation Tube (CLICIT) at the Oregon State University Triga reactor for 50 h. On the basis of previous work, corrections for undesirable neutron-induced reactions on ^{40}K and ^{40}Ca are as follows: $[^{40}Ar/^{39}Ar]_K = 0.00086$; $[^{36}Ar/^{37}Ar]_{Ca} = 0.000264$; $[^{39}Ar/^{37}Ar]_{Ca} = 0.000673$. The standard mineral used to monitor the neutron fluence was 28.02 ± 0.16 Ma sanidine from the Fish Canyon Tuff (Renne et al., 1998). All ages are calculated using decay constants of Steiger and Jäger (1977) and reported with $\pm 2\sigma$ uncertainties at two different levels. First, uncertainties associated with analytical procedures and standard intercalibration are provided; this level of uncertainty is appropriate when comparing this age to other $^{40}Ar/^{39}Ar$ ages, provided all ages are calculated relative to a common standard age. Second, for the plateau and isochron ages, a fully propagated uncertainty that includes the above errors, plus that associated with uncertainty in the ^{40}K decay constant, is reported; this level of uncertainty is appropriate when comparing this age to independent chronometers, for example U–Pb zircon ages (Renne et al., 1998).

A 9-step incremental-heating analysis was performed on a single 1 mg grain of the groundmass using a 25 Watt CO_2 laser at the University of Wisconsin-Madison Rare Gas Geochronology Laboratory. Degassing, clean-up, mass spectrometry, blank corrections and age calculation procedures followed Davidson et al. (2003) and Singer and Brown (2002).

6.2. $^{40}Ar/^{39}Ar$ results

The age spectrum is discordant with apparent ages ranging from 253.7 ± 76.5 to 184.4 ± 2.1 Ma (Table 2; Fig. 13). After decreasing in apparent age over the first 4 increments, the remaining five increments yield an age plateau comprising 70.4% of the ^{39}Ar released with a weighted mean age of 186.3 ± 1.2 Ma with an MSWD

Table 2
Complete $^{40}Ar/^{39}Ar$ incremental heating results of Tuli basalt, Zimbabwe

Laser power (W)		$^{40}Ar/^{39}Ar$	$^{37}Ar/^{39}Ar^{a}$	$^{36}Ar/^{39}Ar$	^{40}Ar (10^{-14} mol)	$^{40}Ar^{*}$ %	K/Ca	^{39}Ar%	Apparent age (Ma) ± 2σ
		200 mg	$J = 0.0134 \pm 0.07\%$		$\mu = 1.0021$	Total gas age = 190.86 ± 1.51			
0.06		19.8196	0.5511	0.0291	0.03	56.78	0.78	0.4	253.68 ± 76.51
0.08		30.8054	0.3030	0.0780	0.05	25.27	1.42	1.1	179.18 ± 39.95
0.10		30.0366	0.3879	0.0698	0.18	31.40	1.11	3.4	214.89 ± 24.68
0.14		12.4455	0.3213	0.0128	1.20	69.70	1.34	24.7	198.58 ± 2.55
0.20	>	9.0833	0.3228	0.0032	1.53	89.77	1.33	33.4	187.26 ± 1.83
0.25	>	8.2194	0.2334	0.0004	1.07	98.92	1.84	23.3	186.74 ± 1.76
0.33	>	8.1330	0.3134	0.0002	0.39	99.43	1.37	8.7	185.78 ± 4.45
0.45	>	8.0008	4.4992	0.0010	0.17	99.99	0.10	3.8	184.39 ± 2.07
0.73	>	8.3953	10.6667	0.0034	0.06	97.82	0.04	1.3	189.79 ± 26.23
		Weighted mean plateau age: 186.26 ± 1.19 Ma				Isochron age: 186.6 ± 1.86 Ma			

Ages calculated relative to 28.02 Ma FCs standard, only analytical and intercalibration uncertainties shown.

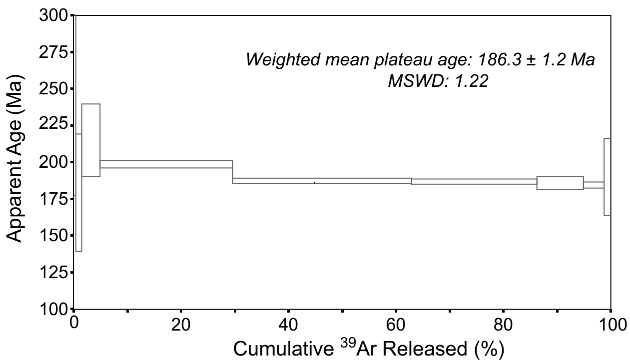

Fig. 13. New $^{40}Ar/^{39}Ar$ plateau age of the Tuli basalt based on a sample collected 50 cm above the contact with the underlying Samkoto Formation. After decreasing in apparent age over the first 4 increments of the analysis, the remaining five increments yield an age plateau comprising 70.4% of the ^{39}Ar released with a weighted mean age of 186.3 ± 1.2 Ma.

of 1.22 (Fig. 13). The inverse isochron defined by the five plateau increments is 186.6 ± 1.9 Ma with an MSWD of 0.06 and a $^{40}Ar/^{36}Ar$ intercept value of 306.2 ± 40.0 that is not different than atmosphere (Table 2). Using a fully propagated uncertainty, the plateau and isochron ages are 186.3 ± 1.2 and 186.6 ± 2.0 Ma, respectively. Since there is no evidence for excess argon, the plateau age is taken as the most precise estimate of time since eruption of the Tuli basalt.

This new age of 186.3 ± 1.2 Ma is comparable to several $^{40}Ar/^{39}Ar$ plateau ages reported for the basalts of the Drakensberg Group of South Africa (Duncan et al., 1997), provided the latter are compared with $\pm 2\sigma$ uncertainties. Interestingly, the age reported here falls very early in the proposed chronology of Karoo igneous activity (Duncan et al., 1997; Jones et al., 2001; Le Gall et al., 2002), and it hints at the possibility of an early eruptive phase in the Tuli Basin. However, additional ages from additional localities are certainly needed before the regional eruptive history in the Tuli Basin can be accurately reconstructed.

7. Conclusions

This report documents the sedimentology and taphonomy of the Mpandi Formation (=Elliot Formation in main Karoo Basin), which is the only Karoo-equivalent unit in the Zimbabwean portion of the Tuli Basin known to preserve dinosaur body fossils. Exposures of the Mpandi Formation show abundant indication of deposition in fluvial and floodplain settings subject to a semi-arid palaeoclimate. These alluvial facies preserve skeletal remains of the prosauropod *Massospondylus*, along with rare indications of other tetrapod taxa (see Munyikwa, 1997, for a faunal overview). The vast majority of localities preserve disarticulated elements of isolated individuals, although rare articulated specimens do occur.

An unconformity separates the Mpandi Formation from the overlying Samkoto Formation (=Clarens Formation in main Karoo Basin). This through-going surface, which can be mapped for ~20 km along exposures that parallel the Limpopo River, rests upon a laterally-continuous zone of pervasive silicification interpreted as a silcrete. This association should come as no surprise, because subaerial unconformities are often found intercalated above authigenic silica horizons (Bain and Ulrich, 1905; Leith, 1925; Smith et al., 1997; Rogers et al., 2001; Hersi et al., 2002). The Mpandi silcrete exhibits morphologic, petrographic, and geochemical traits consistent with intensive leaching near the ground surface during prolonged hiatus. Translocation of most elements resulted in the relative enrichment of silica, which precipitated in a variety of forms and replaced the bulk of the host sediment. Erosion followed, and chert clasts reworked from the silcrete are intercalated at the base of the overlying Samkoto Formation, indicating that the silcrete was in place prior to the resumption of deposition.

The Tuli basalts cap Samkoto deposits, and a new $^{40}Ar/^{39}Ar$ age for these basalts (186.3 ± 1.2 Ma) suggests that they were potentially emplaced near the beginning of Karoo igneous activity. However, it is fully recognized that more ages from additional localities are needed to test this hypothesis. The formative implications of the Mpandi silcrete and associated unconformity, in conjunction with a new radioisotopic age, provide important new insights into the geological history of the region. The unconformity and underlying silcrete also provide great potential for stratigraphic analysis and long-range correlation within the Tuli Basin, and perhaps with other Karoo depocentres in southern Africa.

Acknowledgments

Sincere thanks go to Vanessa, Digby, Adam, and Tarquin Bristow of Sentinel Ranch for graciously permitting access to their land during the midst of safari season. Field research was funded by the National Geographic Society (NGS GRANT 6528-98) and Macalester College (Keck Faculty-Student Research and Beltmann research grants). The National Museum of Natural History in Bulawayo provided field equipment and a vehicle. Analytical work at Macalester College was facilitated by the efforts of J. Thole and K. Wirth. Radioisotopic analyses were made possible by a National Science Foundation technician support grant (EAR-0114055) to B. Singer. Melissa Harper and Brian Jicha (University of Wisconsin) helped to prepare and run the Tuli basalt sample. Insightful comments and suggestions by E. Bordy and O. Catuneanu are greatly appreciated.

References

Aldiss, D.T., Benson, J.M., Rundle, C.C., 1984. Early Jurassic pillow lavas and palynomorphs in the Karoo of eastern Botswana. Nature 310, 302–304.

Bain, H.F., Ulrich, E.O., 1905. Copper deposits of Missouri. United States Geological Survey Bulletin 267, 50.

Bordy, E.M., 2000. Sedimentology of the Karoo Supergroup in the Tuli Basin (Limpopo River area, South Africa). Ph.D. thesis, Rhodes University, South Africa, p. 266.

Bordy, E.M., Catuneanu, O., 2001. Sedimentology of the upper Karoo fluvial strata in the Tuli Basin, South Africa. Journal of African Earth Sciences 33, 605–629.

Bordy, E.M., Catuneanu, O., 2002a. Sedimentology and palaeontology of upper Karoo aeolian strata (Early Jurassic) in the Tuli Basin, South Africa. Journal of African Earth Sciences 35, 301–314.

Bordy, E.M., Catuneanu, O., 2002b. Sedimentology of the lower Karoo Supergroup fluvial strata in the Tuli Basin, South Africa. Journal of African Earth Sciences 35, 503–521.

Bordy, E.M., Catuneanu, O., 2002c. Sedimentology of the Beaufort-Molteno Karoo fluvial strata in the Tuli Basin, South Africa. South African Journal of Geology 105, 51–66.

Bordy, E.M., Hancox, P.J., Rubidge, B.S., 2004. Fluvial style variations in the Late Triassic–Early Jurassic Elliot Formation, main Karoo Basin, South Africa. Journal of African Earth Sciences 38, 383–400.

Broom, R., 1912. On the remains of the theropodous dinosaur from the northern Transvaal. Transactions of the Geological Society of South Africa 14, 82–83.

Burke, K.C.A., Dewey, J.F., 1973. Plume-generated triple junctions: key indicators in applying plate tectonics to old rocks. Journal of Geology 86, 406–433.

Catuneanu, O., Hancox, P.J., Rubidge, B.S., 1998. Reciprocal flexural behaviour and contrasting stratigraphies: a new basin development model for the Karoo retroarc foreland system, South Africa. Basin Research 10, 417–439.

Catuneanu, O., Kun-Jager, E.M., Rubidge, B.S., Hancox, P.J., 1999. Lateral changes of the Dwyka facies: implications for the initiation of the Cape Orogeny and the associated Karoo foreland system. In: Abstracts of Proceedings, American Association of Petroleum Geologists Annual Meeting, April 11–14, San Antonio, TX, p. A22.

Cooper, M.R., 1980. The first record of the prosauropod dinosaur *Euskelosaurus* from Zimbabwe. Arnoldia Zimbabwe 9, 1–17.

Davidson, C., Davis, K.J., Bailey, C.M., Tape, C.H., Singleton, J., Singer, B.S., 2003. Age, origin, and significance of brittle faulting and pseudotachylyte along the Coast shear zone, Prince Rupert, British Columbia. Geology 31, 43–46.

Dingle, R.V., Siesser, W.G., Newton, A.R., 1983. Mesozoic and Tertiary Geology of Southern Africa. A.A. Balkema Publishers, Rotterdam, Netherlands, p. 385.

Duncan, R.A., Hooper, P.R., Rehacek, J., Marsh, J.S., Duncan, A.R., 1997. The timing and duration of the Karoo igneous event, southern Gondwana. Journal of Geophysical Research 102, 18127–18138.

Geological Survey of Rhodesia, 1974. Mazunga and Tuli Sheets (1:100,000). Geological Survey of Rhodesia Short Report No. 40. Thompson, A.O., 1975.

Grant, K., Aitchison, G., 1970. The engineering significance of silcretes and ferricretes in Australia. Engineering Geology 4, 93–120.

Hancox, P.J., Rubidge, B.S., 1997. The role of fossils in interpreting the development of the Karoo Basin. Palaeontologia Africana 33, 43–56.

Haughton, S.H., 1924. The fauna and stratigraphy of the Stormberg Series. Annals of the South African Museum 12 (8), 323–497.

Hersi, O.S., Lavoie, D., Mohamed, A.H., Nowlan, G.S., 2002. Subaerial unconformity at the Potsdam–Beekmantown contact in the Quebec Reentrant; regional significance of the Laurentian continental margin history. Bulletin of Canadian Petroleum Geology 50, 419–440.

Johnson, M.R. (Ed.), 1994. Lexicon of South African Stratigraphy. Part 1. Phanerozoic Units. Pretoria: SACS, Council for Geoscience, Berlin, p. 56.

Johnson, M.R., van Vuuren, C.J., Hegenberger, W.F., Key, R., Shoko, U., 1996. Stratigraphy of the Karoo Supergroup in southern Africa: an overview. Journal of African Earth Sciences 23, 3–15.

Johnson, M.R., Van Vuuren, C.J., Visser, J.N.J., Cole, D.I., Wickens, H.de.V., Cristie, A.D.M., Roberts, D.L., 1997. The Foreland Karoo Basin, South Africa. In: Selley, R.C. (Ed.), African Basins, Sedimentary Basins of the World, vol. 3. Elsevier Science B.V., Amsterdam, pp. 269–317.

Jones, D.L., Duncan, R.A., Briden, J.C., Randall, D.E., MacNiocaill, C., 2001. Age of the Batoka basalts, northern Zimbabwe, and the duration of the Karoo Large Igneous Province magmatism. Geochemistry Geophysics Geosystems 2, 1–15.

Kitching, J.W., 1977. The distribution of the Karoo vertebrate fauna. Memoir of the Bernard Price Institute for Palaeontological Research 1, 131.

Kitching, J.W., Raath, M.A., 1984. Fossils from the Elliot and Clarens formations (Karoo Sequence) of the northeastern Cape, Orange Free State and Lesotho, and a suggested biozonation based on tetrapods. Palaeontologia Africana 25, 111–125.

Langford-Smith, T., 1978. A select review of silcrete research in Australia. In: Langford-Smith, T. (Ed.), Silcrete in Australia. Australia University of New England, Department of Geography, pp. 1–11.

Le Gall, B., Tshoso, G., Jourdan, F., Féraud, G., Bertrand, H., Tiercelin, J.J., Kampunzu, A.B., Modisi, M.P., Dyment, J., Maia, M., 2002. $^{40}Ar/^{39}Ar$ geochronology and structural data from the giant Okavango and related mafic dyke swarms, Karoo igneous province, northern Botswana. Earth and Planetary Science Letters 202, 595–606.

Leith, C.K., 1925. Silicification of erosion surfaces. Economic Geology 20, 513–523.

Meyer, R., 1997. Paleoalterites and Paleosols: Imprints of Terrestrial Processes in Sedimentary Rocks. A.A. Balkema Publishers, Rotterdam, Netherlands, p. 151.

Milnes, A.R., Thiry, M., 1992. Silcretes. In: Martini, I.P., Chesworth, W. (Eds.), Weathering, Soils and Paleosols. Elsevier Science B.V., Amsterdam, The Netherlands, pp. 349–377.

Munyikwa, D., 1997. Faunal analysis of Karoo-aged sediments in the northern Limpopo Valley, Zimbabwe. Arnoldia Zimbabwe 10, 129–140.

Nash, D., Thomas, D., Shaw, P., 1994. Siliceous duricrusts as palaeoclimate indicators: evidence from the Kalahari Desert of Botswana. Palaeogeography, Palaeoclimatology, Palaeoecology 112, 279–295.

Renne, P.R., Swisher, C.C., Deino, A.L., Karner, D.B., Owens, T.L., DePaolo, D.J., 1998. Intercalibration of standards, absolute ages and uncertainties in $^{40}Ar/^{39}Ar$ dating. Chemical Geology 145, 117–152.

Rogers, R.R., Arcucci, A.B., Abdala, F., Sereno, P.C., Forster, C.A., May, C.L., 2001. Paleoenvironment and taphonomy of the Chañares Formation tetrapod assemblage (Middle Triassic), northwestern Argentina: Spectacular preservation in volcanogenic concretions. Palaios 16, 461–481.

Rubidge, B.S., Johnson, M.R., Kitching, J.W., Smith, R.M.H., Keyser, A.W., Groenewald, G.H., 1995. An introduction to the biozonation of the Beaufort Group. In: Rubidge, B.S. (Ed.), Biostratigraphy of the Beaufort Group (Karoo Supergroup), South Africa. South African Committee for Stratigraphy, Biostratigraphic Series 1, Pretoria, pp. 1–2.

Simon-Coincon, R., Milnes, A., Thiry, M., Wright, M., 1996. Evolution of landscapes in northern South Australia in relation to the distribution and formation of silcretes. Journal of the Geological Society, London 153, 467–480.

Singer, B., Brown, L.L., 2002. The Santa Rosa Event: $^{40}Ar/^{39}Ar$ and paleomagnetic results from the Valles Rhyolite near Jaramillo Creek, Jemez Mountains, New Mexico. Earth and Planetary Science Letters 197, 51–65.

Smith, G.L., Dott Jr., R.H., Byers, C.W., 1997. Authigenic silica fabrics associated with Cambro-Ordovician unconformities in the Upper Midwest. Geoscience Wisconsin 16, 25–36.

Smith, R.M.H., Eriksson, P.G., Botha, W.J., 1993. A review of the stratigraphy and sedimentary environments of the Karoo-aged basins of South Africa. Journal of African Earth Sciences 16, 143–169.

Smith, R.M.H., Kitching, J., 1997. Sedimentology and vertebrate taphonomy of the *Tritylodon* Acme Zone: a reworked paleosol in the Lower Jurassic Elliott Formation, Karoo Supergroup, South Africa. Palaeogeography, Palaeoclimatology, Palaeoecology 131, 29–50.

Steiger, R.H., Jäger, E., 1977. Subcommission on geochronology: convention on the use of decay constants in geo- and cosmochronology. Earth and Planetary Science Letters 5, 320–324.

Summerfield, M.A., 1983a. Petrography and diagenesis of silcrete from the Kalahari Basin and Cape Coastal Zone, southern Africa. Journal of Sedimentary Petrology 53, 895–909.

Summerfield, M.A., 1983b. Silcrete. In: Gouide, A.S., Pye, K. (Eds.), Chemical Sediments and Geomorphology. Academic Press, London, pp. 59–91.

Terry, R.C., 2001. Character and significance of a silicified unconformity in Late-Triassic–Early Jurassic strata of the Limpopo Valley, southern Zimbabwe. Senior Honors Thesis, Macalester College, Saint Paul, Minnesota, USA, p. 123.

Terry, R.C., Rogers, R.R., Wirth, K.R., 2001. Character and origin of the Mpandi silcrete (Early Jurassic?), Limpopo Valley, Zimbabwe. Abstracts with Programs. Geological Society of America 33 (6), 446.

Thiry, M., 1999. Diversity of continental silicification features: examples from the Cenozoic deposits of the Paris Basin and neighbouring basement. Special Publication of the International Association of Sedimentologists 27, 87–127.

Thompson, A.O., 1975. The Karoo rocks in the Mazunga Area, Beitbridge District. Short Report No. 40, Rhodesia Geological Survey, p. 79.

Ullyott, J., Nash, D., Shaw, P., 1998. Recent advances in silcrete research and their implications for the origin and palaeoenvironmental significance of sarsens. Proceedings of the Geologists' Association 109, 255–270.

Vail, V.R., Hornung, G., Cox, K.G., 1969. Karoo basalts of Tuli, Rhodesia. Bulletin of Volcanology 33, 398–418.

Webb, J.A., Golding, S.D., 1998. Geochemical mass-balance and oxygen-isotope constraints on silcrete formation and its paleoclimatic implications in southern Australia. Journal of Sedimentary Research 68, 981–993.